6D.1 DISTRIBUTIONS OF CONVECTION IN RAPIDLY INTENSIFYING TROPICAL CYCLONES

Cheng Tao* and Haiyan Jiang
Department of Earth & Environment, Florida International University, Miami, FL

1. INTRODUCTION

The structure and intensity changes of tropical cyclones (TCs) are affected by a combination of internal dynamical processes and the storm's interaction with both the underlying ocean and its atmospheric environment (Wang and Wu 2004). One of the important internal dynamical processes for TC evolution is the asymmetric deep convection (Hendricks 2012). Observational studies have linked TC intensity change to the occurrence of deep convection in terms of associated enhanced latent heat release and subsidence in the storm core, and increased vertical mass flux in the eyewall (Reasor et al. 2009; Rogers 2010), while modeling studies have highlighted the role of rotating deep convection (termed vortical hot towers, Montgomery and Smith 2011).

A portion of the latent heat released in the asymmetric convection is transformed into symmetric kinetic energy (KE) and available potential energy (APE) of the storms (Nolan et al. 2007). It is suggested that the intensity of a vortex changes as a symmetric response to the azimuthally averaged heating (Nolan and Grasso, 2003). This implies that whether the latent heat associated with asymmetric deep convection is strong enough to increase the azimuthally average heating is critical in determining the occurrence of intensification. The location of the heating is also important. Heating inside the radius of maximum winds (RMW) has higher kinetic energy efficiency (Schubert and Vigh 2008).

**Corresponding author address*: Cheng Tao, Dept. of Earth & Environment, Florida International University, Miami, FL 33199.
E-mail: ctao003@fiu.edu

Convection and precipitation fields are a reasonable indication of the horizontal distribution of the latent heating and are primarily dominated by the environmental vertical wind shear (Corbosiero and Molinari 2002; Reasor et al. 2013). Using 14 years of Tropical Rainfall Measuring Mission (TRMM) Precipitation Radar (PR) overpasses, Zagrodnik and Jiang (2014) studied the distributions of precipitation, convection and latent heating in rapidly intensifying TCs and concluded that the distribution of latent heating in RI is less asymmetric than non-RI storms. Based on the same database, distributions of four groups of convection (defined with 20-dBZ radar echo) in rapidly intensifying TCs are examined in this study, with an emphasis on their contribution to total volumetric rain.

2. DATA AND METHODOLOGY

We use the dataset provided by Zagrodnik and Jiang (2014), which is derived from the TRMM Tropical Cyclone Precipitation Feature (TCPF) database (Jiang et al. 2011). The version 7 PR 2A25 is applied to obtain a 3D view of the reflectivity structure of TCs (Kummerow et al. 1998). From 1998 to 2011, 818 northern hemisphere tropical storms through category 2 hurricanes with at least moderately favorable environmental conditions are included in this study. Each overpass is manually selected to ensure that at least some portion of the center or near-center area is captured.

Based on the difference between the current and future 24-h intensity, overpasses are classified into weakening (W), neutral

(N), slowly intensifying (SI) and rapidly intensifying (RI, Table 1). However, a RI event can continue for as long as 48-60 hours, indicating that the time of the overpass does not necessarily correspond to the onset of a RI event. Therefore, the RI storms are subdivided into RI initial and RI continuing (Table 2). RI initial is regarded as important in TC intensity forecast since it is near the onset of an RI event.

Table 1. Definition of intensity change categories and the sample size of selected PR overpasses. V_{max+24} represent the maximum surface wind speed in the future 24-h.

Category	Max. wind speed range (kt)	PR overpasses
W	$V_{max+24} - V_{max} \leq -10$	136
N	$-10 < V_{max+24} - V_{max} < 10$	329
SI	$10 \leq V_{max+24} - V_{max} < 30$	250
RI	$V_{max+24} - V_{max} \geq 30$	103
Total		**818**

Table 2. Definition of initial and continuing rapid intensification and the number of sampled PR overpasses.

Category	Max. wind speed range (kt)	PR overpasses
RI init.	$V_{max+12} - V_{max-12} < 30$ & $V_{max} - V_{max-24} < 30$	46
RI cont.	$V_{max+12} - V_{max-12} \geq 30$ or $V_{max} - V_{max-24} \geq 30$	57
RI total	$V_{max+24} - V_{max} \geq 30$	**103**

Kieper and Jiang (2012) argued that a precipitative ring feature on the Naval Research Laboratory (NRL) 37 GHz color image is associated with RI. The ring feature occurs in the inner core region prior to RI and mainly consists of shallow precipitation, with asymmetric deep convection embedded. To study the relative importance of shallow convection versus very deep convection in RI, four groups of convection is defined according to the height of 20 dBZ radar echo from TRMM PR (Z_{20dBZ}). These include shallow convection (Z_{20dBZ} <4km), moderate convection (10km>Z_{20dBZ}≥4km), moderately deep convection (14km>Z_{20dBZ} ≥10km), and very deep convection (Z_{20dBZ}≥14km).

Three variables are selected, including the percent occurrence of convection (%), total volumetric rain ($mmhr^{-1}km^2$) and convection contribution to total volumetric rain (%). We use composite images to display the shear-directed distributions of convection in TCs. Here, the vertical wind shear is calculated by averaging the 200-hPa and 850-hPa wind vectors from the European Center for Mid-Range Weather Forecasting (ECMWF) interim reanalysis dataset within a ring of 500-750 km from the center (Simmons et al. 2006). To generate the images, the selected overpasses are first rotated with the vertical wind shear pointing upward and the center in the middle. The PR pixels, with their new coordinates relative to the center and vertical wind shear, are then compiled into a 10×10 km grid box. So each grid point represents the composite-mean values of total pixels within the 100 km^2 box from all overpasses.

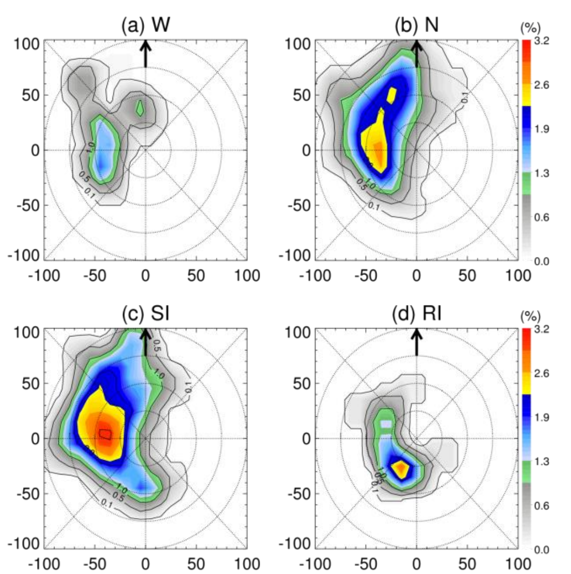

Fig. 1. Composite shear-relative distribution of the percent occurrence of very deep convection for (a) W, (b) N, (c) SI, and (d) RI. The black arrow represents the direction of the vertical wind shear vector. The 25, 50, 75, and 100 km radii are shown as dotted rings.

3. RESULTS

3.1 Percent occurrence of convection

Composite shear-relative distributions of percent occurrence of very deep, moderately deep, moderate and shallow convection are shown in Fig 1-4. According to the direction of vertical wind shear, the upper-left, upper-right, lower-left, and lower-right quadrant is referred to as downshear-left, downshear-right, upshear-left, and upshear-right, respectively (Chen et al. 2006).

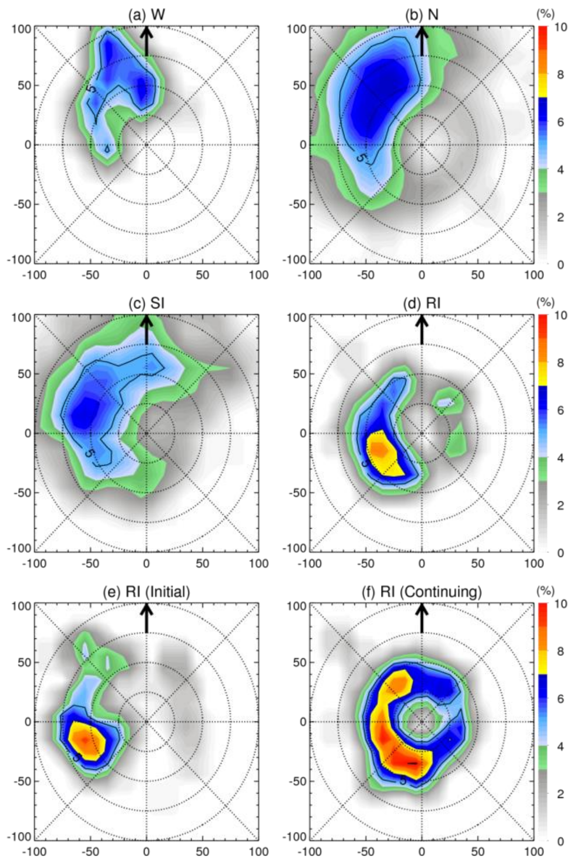

Fig. 2. Composite shear-relative distribution of the percent occurrence of moderately deep convection for (a) W, (b) N, (c) SI, (d) RI, (e) RI initial, and (f) RI continuing.

Very deep convection is quite rare in TCs, with the maximum percent occurrence at about 3% (Fig. 1). Due to the limited sample size, RI cases are not further grouped into RI initial and RI continuing. Although very deep convection is less widespread in RI than non-RI storms, it does concentrate in the innermost 50 km where it is especially efficient at strengthening the vortex. The downshear-left quadrant is favored for W, N and SI in the maximum percent coverage of moderately deep convection (Fig. 2); while in RI, the maximum is centered in upshear-left and located much closer to the center. RI initial has significantly greater moderately deep convection than SI in the upshear-left quadrant. An eyewall feature is seen in RI continuing storms.

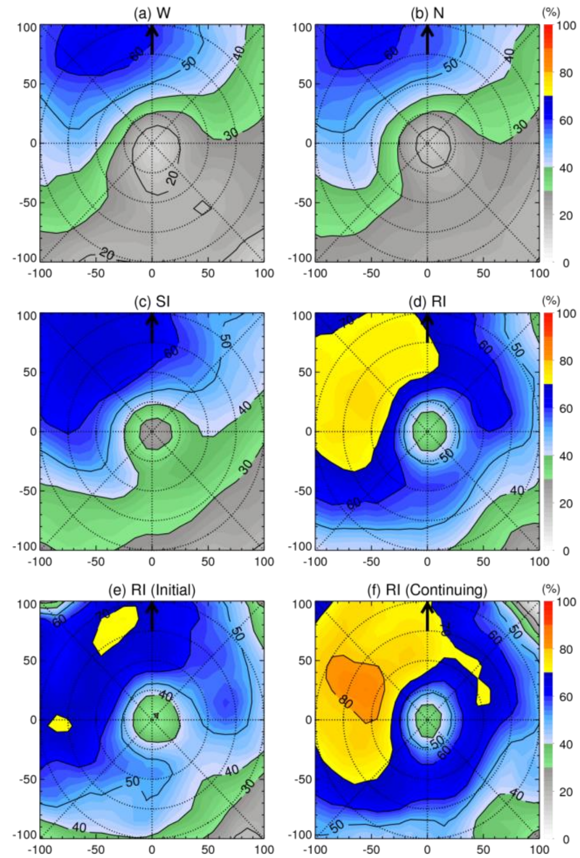

Fig. 3. Same as Fig. 2, except for moderate convection.

The downshear-left quadrant is favored in all cases for the greatest percent occurrence of moderate convection (Fig. 3). A similar pattern is observed for W and N storms and it is more asymmetric than SI and RI, as the maximum is 60-70% in downshear-left but 20% in upshear-right. Significant difference is found between SI and RI initial storms in the upshear semicircle. Fig. 4 shows a very asymmetric pattern in W storms for the percent occurrence of shallow convection, as the maximum is 10-15% downshear-left and <5% upshear-right. A ring of 5% shallow convection wraps around the center in RI initial, which is similar to the ring feature indicated by Kieper and Jiang (2012). The frequency of shallow convection decreases rapidly in RI continuing. It is suggested that storms prior to RI are firstly covered with significantly increased shallow convection.

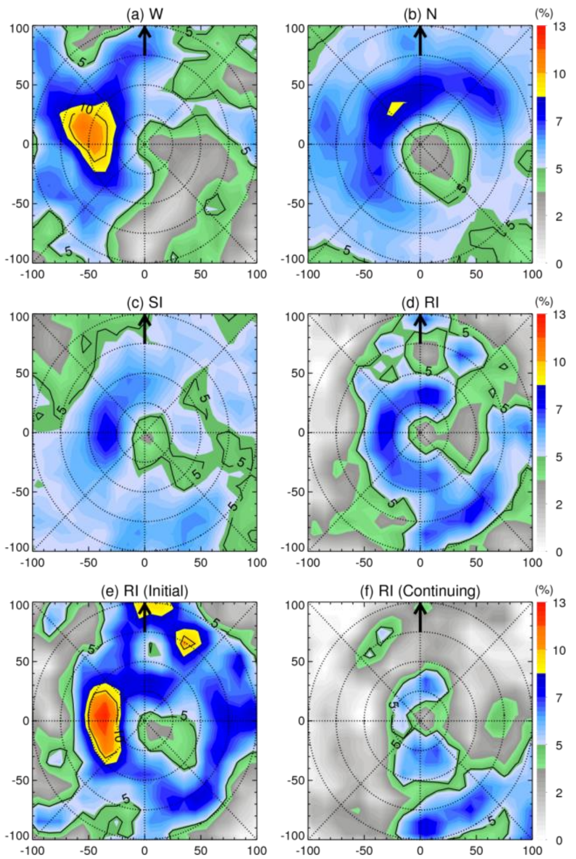

Fig. 4. Same as Fig. 3, except for shallow convection.

3.2 Total volumetric rain

We begin with the radial distribution of total volumetric rain by binning the PR pixels into 5-km annuli in radius around the center. Figure 5 illustrates the azimuthally averaged total volumetric rain outward up to 150 km, corresponding to the inner core and inner rainbands region. Panel (a) shows a similar pattern for W, N and SI while RI has much higher azimuthally averaged rainfall. In the innermost 100 km of the center, the mean difference between SI and RI in total volumetric rain is about 18.66 mmhr^{-1}km^{2} and is significant at the 99% confidence level (Table 3). Panel (b) further indicates that it is RI continuing that accounts for the pronounced difference between SI and RI in total volumetric rain, as the curves for RI initial and SI are very similar.

Table 3. Mean values of total volumetric rain in each shear-relative quadrant within the innermost 100 km.

Category	DR	UR	UL	DL	Total
W	50.7	19.4	46.9	112.7	63.7
N	50.1	22.5	44.0	106.5	61.8
SI	66.1	29.7	50.8	117.9	73.9
RI	74.2	53.0	94.1	117.5	92.6
RI init.	68.8	37.3	73.0	107.6	74.3
RI cont.	78.6	65.72	*111.1*	125.6	107.3
All	58.1	28	52.9	112.4	69.7

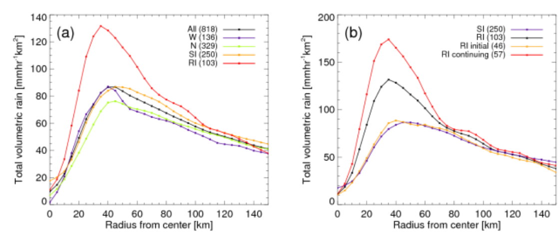

Fig. 5. Line plots of azimuthally averaged total volumetric rain, organized by the total sample (black line) and the intensity change categories (colored lines).

The corresponding composite shear-relative distribution (not shown) is closely analogous to the mean rain rates in Figures 16-18 of Wingo and Cecil (2009), as the precipitation is displaced downshear and to the left of the shear vector. The maximum total volumetric rain occurs in downshear-left in all intensity change categories but RI storms have a more symmetric pattern. RI initial storms present much greater total volumetric rain than SI in upshear-left, with the quadrant-mean difference within the innermost 100 km about 22.15 mmhr^{-1}km^{2} and significant at the 90% confidence level (Table 3).

3.3 Convection contribution to total volumetric rain

Table 4 shows mean values of convection contribution to total volumetric rain, which is averaged within the innermost 100 km. Moderate convection accounts for about 75% of total volumetric rain while the other three groups of convection together account for 25%. The percentage of total rainfall from moderate convection is about 15.1, 7.0 and 8.2 times greater than very deep, moderately deep and shallow convection, respectively.

Table 4. Mean values of convection contribution to total volumetric rain. Averaged within the innermost 100 km.

Category	Very deep	Moderately deep	Moderate	Shallow
W	3.96	9.54	72.80	11.49
N	5.18	10.94	70.72	11.62
SI	5.84	10.53	76.15	6.33
RI	3.15	11.23	81.61	3.76
RI init.	-	10.90	81.11	4.31
RI cont.	-	11.49	82.02	3.31
Total	4.92	10.62	74.10	8.99

Despite of rare occurrence, very deep convection accounts for a disproportionate amount to total volumetric rain. Within the innermost 100 km, less than 1% of total pixels have 14 km reflectivity ≥ 20 dBZ but these pixels contribute about 5% to total rainfall. The corresponding composite shear-relative distribution shows that upshear-left is favored in all intensity change categories for the maximum convection contribution to total volumetric rain (not shown). RI has the lowest percentage of total volumetric rain from very deep convection, with the mean difference between SI and RI about 3% and significant at the 99% confidence level.

Moderately deep convection accounts for greater total volumetric rain in RI than SI. Corresponding shear-relative distribution (not shown) illustrates that W and N storms have the maximum convection contribution to total rainfall in downshear-left while SI and RI have the maximum centered in upshear-left and displaced closer to the center. In RI continuing, downshear-left still has the highest percentage, peaking at 25-30%, but the overall appearance is more symmetric.

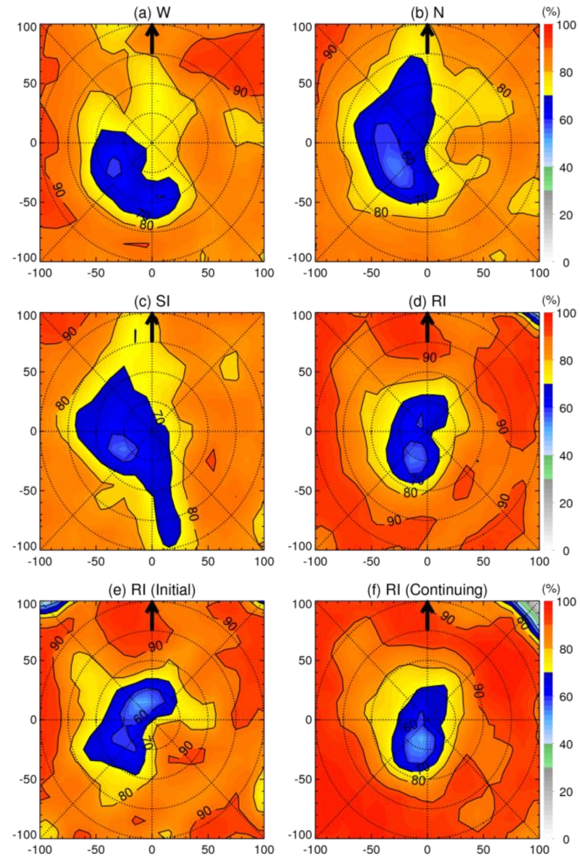

Fig 6. Composite shear-relative distribution of contribution of very deep convection to total volumetric rain for (a) W, (b) N, (c) SI, (d) RI, (e) RI initial, and (f) RI continuing.

Moderate convection accounts for over 80% of total volumetric rain in RI storms. The mean difference between SI and RI is ~5.5%, which is significant at the 95% confidence level (Table 4). Furthermore, a pronounced difference (about 5.0%) is observed between SI and RI initial, which is significant at the 90% confidence level. Corresponding shear-relative distribution in Figure 6 illustrates a large area of > 90% total volumetric rain from moderate convection in RI than non-RI storms. A ring of > 90% extends completely around the center in RI continuing storms.

About 9% of total volumetric rain is from shallow convection. It should be noted that the definition of shallow convection in this study does not contain any ice phase. Thus, the rain rate of shallow convection may be underestimated due to the TRMM PR 2A25 algorithm. The shear-relative distribution illustrates that upshear-right is favored in all intensity change categories except W for the maximum convection contribution to rainfall. SI storms have higher percentage of total rainfall from shallow convection compared with RI, although the convection coverage is similar for SI and RI. In the innermost 50 km, however, RI initial presents greater total rainfall from shallow convection than SI.

4. CONCLUSION

Very deep convection (defined as 20 dBZ radar echo $\geq$ 14 km) is less widespread in RI than non-RI storms but it does concentrate in the innermost 50 km within a region of high kinetic energy efficiency. TCs prior to RI are first covered with increased moderate convection (20dBZ radar echo between 4-10 km) and shallow convection (20dBZ radar echo<4km), and then moderately deep convection (20dBZ radar echo between 10-14km). A ring of > 5% coverage of shallow convection, similar to the 37 GHz ring feature in Kieper and Jiang (2012), is observed in RI initial storms.

RI presents greater and more symmetric total volumetric rain than other intensity change categories, consistent with previous studies that RI storms have widespread precipitation with high total volumetric rain in the inner core region (e.g., Jiang and Ramirez, 2013). Statistical analysis suggests an important role of moderate convection in RI, as it contributes about 75% of total volumetric rain, providing sufficient energy for TC development.

5. ACKNOWLEDGEMENTS

The authors would like to acknowledge Joseph P. Zagrodnik for the construction of the dataset, and Drs. Tie Yuan and Chuntao Liu for helping on TRMM data processing. The first author received support from NASA Earth and Space Science Fellowship (NESSF) award (#NNX11AL66H).

6. REFERENCE

Chen, S. S., J. A. Knaff, F. D. Marks, 2006: Effects of vertical wind shear and storm motion on tropical cyclone rainfall asymmetries deduced from TRMM. *Mon. Wea. Rev.*, **134,** 3190-3208.

Corbosiero, K. L., and J. Molinari, 2002: The effects of vertical wind shear on the distribution of convection in tropical cyclones. *Mon. Wea. Rev.*, **130,** 2110-2123.

Hendricks, E. A., 2012: Internal dynamical control on tropical cyclone intensity variability. *Trop. Cyclone Res. Rev.*, **1,** 97-105.

Jiang, H., and E. M. Ramirez, 2013: Necessary conditions for tropical cyclone rapid intensification as derived from 11 years of TRMM data. *J. Climate.*, **26,** 6459-6470.

——, C. Liu, and E. J. Zipser, 2011: A TRMM-based Tropical Cyclone Cloud and Precipitation Feature Database. *J. Appl. Meteor. Climatol.*, **50,** 1255-1274.

Kieper, M., and H. Jiang, 2012: Predicting tropical cyclone rapid intensification using the 37GHz ring pattern identified from passive microwave measurements. *Geophys. Res. Lett.*, **39,** L13804.

Montgomery, M. T., and R. K. Smith, 2011: Paradigms for tropical cyclone intensification. *Quart. J. Roy. Meteor. Soc.*, **137,** 1-31.

Nolan, D.S., and L.D. Grasso, 2003: Three-dimensional, nonhydrostatic perturbations to balanced, hurricane-like vortices. Part II: Symmetric response and nonlinear simulations. *J. Atmos. Sci.*, **60,** 2717-2745.

——, Y. Moon, and D.P.Stern, 2007: Tropical cyclone intensification from asymmetric convection: Energetics and efficiency. *J. Atmos. Sci.*, **64,** 3377-3405.

Reasor, P. D., M. Eastin, and J. F. Gamache, 2009: Rapidly intensifying Hurricane Guillermo (1997). Part I. Low-wavenumber structure and evolution. *Mon. Wea. Rev.*, **137,** 603-631.

——, R. Rogers, and S. Lorsolo, 2013: Environmental flow impacts on tropical cyclone structure diagnosed from airborne Doppler radar composites. *Mon. Wea. Rev.*, **141,** 2949-2969.

Rogers, R., 2010: Convective-scale structure and evolution during a high-resolution simulation of tropical cyclone rapid intensification. *J. Atmos. Sci.*, **67,** 44-70.

Schubert, W. H., and J. S. Vigh: 2008: Rapid development of the tropical cyclone warm core. Preprints, *28th Conf. on Hurricanes and Tropical Meteorology,* Orlando, FL, Amer. Meteor. Soc., 14C.3.

Wang, Y., and C.-C. Wu, 2004: Current understanding of tropical cyclone structure and intensity changes – a review. *Meteorol Atmos Phys,* **87,** 257-278.

Wingo, Matthew T., Daniel J. Cecil, 2010: Effects of vertical wind shear on tropical cyclone precipitation. *Mon. Wea. Rev.*, **138,** 645–662.

Zagrodnik, P. J., and H. Jiang, 2014: Rainfall, convection, and latent heating distributions in rapidly intensifying tropical cyclones. *J. Atmos. Sci.*, first revision submitted.